Flow-fiber coupled viscosity in injection molding simulations of short fiber reinforced thermoplastics

Tianyi Li, Jean-François Luyé

Flow-fiber coupled viscosity in injection molding simulations of short fiber reinforced thermoplastics

Tianyi Li[a,*], Jean-François Luyé[a]

[a]*Promold, 43 rue Boursault, 75017 Paris, France*

Abstract

The main objective of this communication is to numerically investigate the use of fiber-dependent viscosity models in injection molding simulations of short fiber reinforced thermoplastics with a latest commercial software (Moldflow Insight 2018). We propose to use the homogenization-based Lipscomb's model to take into account possible flow-fiber coupling effects. The original model is adapted and then implemented in the Moldflow Insight API framework. Numerical simulations are performed in a test-case rectangle flat plate geometry with two latest fiber orientation models. The resulting coupled flow kinematics and fiber evolutions are then compared to the standard uncoupled simulations. Interpretations are given based on detailed post-processing of the field results. Certain deformation conditions are expected to be better taken into account, which may also in return lead to an improved fiber orientation prediction.

Keywords: Injection molding, Fibers, Rheological properties, Process Simulation

1. Introduction

Short fiber reinforced thermoplastics are gaining popularity in industries because they can guarantee mechanical resistance specifications while achieving overall part weight reductions. Integrative simulation procedures Adam and Assaker (2014) are extremely appealing since heterogeneous local microstructure information caused by different processing steps can then be transferred to the subsequent mechanical simulations. In particular, fiber-induced material anisotropy well placed in some critical loaded regions can be better taken into account, resulting in an even optimized part design.

An experimentally validated injection molding simulation constitutes hence the cornerstone of these integrated simulations of injected short fiber reinforced thermoplastics. It is now well known that an inaccurate prediction of fiber orientation distribution in the part could affect ultimate structural response simulations via finite element analyses, see Wedgewood et al. (2017). According to Rolland et al. (2016), a well predicted injection molding induced skin-shell-core fiber orientation structure (cf. Papathanasiou (1997)) is also crucial since it contributes to a correct prediction of damaging mechanism and ultimate failure of these composites.

It is discovered that the fiber orientation models currently available in commercial softwares produce often unsatisfactory predictions in the core region, see Kleindel et al. (2015); Tseng et al. (2017). Compared to experimental results, fibers are estimated to be over-aligned in the flow direction on the mid-surface and the width of the core is also under predicted. Since the core region is in general dominated by divergent

*Corresponding author

Email addresses: tianyi.li@promold.fr (Tianyi Li), jfluye@promold.fr (Jean-François Luyé)

flows toward the transverse direction, it can be argued that these elongational deformations are not correctly taken into account in current models and a flow-fiber coupled simulation with fiber-dependent rheological properties may be more appropriate, cf. Tucker (1991).

There exists already a relatively abundant literature on different flow-induced rheological models, see Phan-Thien and Zheng (1997) for instance for a quick review. The basic idea is that under shear flows fibers contribute less to the overall suspension viscosity when they are aligned to the shear direction, while it is the opposite for elongational flows in the same direction, cf. Laun (1984). Since, these fiber-dependent viscosity models have been applied to flow and injection molding simulations, see for instance Ranganathan and Advani (1993); Verweyst and Tucker (2002); Vincent et al. (2005); Redjeb et al. (2006); Mazahir et al. (2013); Costa et al. (2015); Tseng et al. (2017). The research is still on-going and no definite conclusions have been yet reached on whether or not these flow-fiber coupling effects are really important for most cases. That's probably one of the reasons why currently almost all commercial injection molding softwares still perform an uncoupled analysis.

The objective of this paper is thus to present some updated results on the subject with a latest injection molding software (Moldflow Insight 2018). Thanks to its API framework Costa et al. (2015), in Section 2 a representative anisotropic fiber-induced viscosity model is implemented as a user-defined viscosity function. In particular, fiber orientation is explicitly taken into account in the viscosity. Compared to some previous researches, in Section 3 the flow-fiber coupling effects are numerically evaluated by using more physical injection conditions via non-isothermal three-dimensional finite element computations. Furthermore two latest experimentally validated fiber orientation models (RSC and MRD) are also compared in terms of their possible different contributions to the overall coupling. Conclusions and future research directions drawn from the numerical results are indicated in Section 4.

2. Flow-fiber coupled viscosity models

2.1. Anisotropic fiber-induced viscosity via Lipscomb's model

For (short) fiber reinforced thermoplastics (that is, when the immersed particle aspect ratio r is sufficiently large, say $r > 20$, which is generally satisfied by fibers), the anisotropy induced by these fibers on the overall suspension viscosity can be described by the following Lipscomb's model (see Lipscomb et al. (1988); Phan-Thien and Zheng (1997) and references therein for a detailed homogenization-based derivation of similar models)

$$\boldsymbol{\sigma} = -p\mathbf{I} + 2\eta\mathbf{D} + 2\eta N_{\mathrm{p}}\mathbb{A}\mathbf{D}\,, \tag{1}$$

where $\boldsymbol{\sigma}$ is the (macroscopic) stress tensor for the fiber reinforced suspension, p is the pressure, $\mathbf{I}$ is the 2nd order identity tensor, $\mathbf{D} = \frac{1}{2}\,\mathrm{dev}(\nabla\mathbf{v} + \nabla^{\mathsf{T}}\mathbf{v})$ is the deviatoric deformation rate tensor, η refers to the viscosity of the matrix (without fibers) and $\mathbb{A}$ designates the 4th order fiber orientation tensor introduced in Advani and Tucker (1987). Note that according to (1), the viscosity of the suspension is now no longer a scalar but a 4th order tensor

$$\boldsymbol{\sigma} = -p\mathbf{I} + 2\mathbb{V}\mathbf{D} \quad \text{with} \quad \mathbb{V} = \eta(\mathbb{I} + N_{\mathrm{p}}\mathbb{A})\,, \tag{2}$$

with $\mathbb{I}$ the 4th order identity operator.

In (1) and (2), the coefficient N_{p} measures the scalar intensity of the anisotropic contribution of fibers to the overall viscosity. In particular when one sets $N_{\mathrm{p}} = 0$, we retrieve the uncoupled scalar viscosity model, completely independent of fiber evolutions during the injection process. In this communication we adopt the functional dependence of N_{p} on fiber aspect ratio and volume fraction proposed by Phan-Thien and Graham (1991), which is particularly suitable for concentrated fiber-reinforced suspensions.

2.2. Adaptation for the Moldflow Insight API framework

In order to evaluate numerically Lipscomb's fiber-induced viscosity model in injection molding simulations, we propose to implement (2) in the Moldflow Insight API framework described in Costa et al. (2015).

Currently, only a *scalar* user-defined viscosity function is supported via this interface. Hence, the original Lipscomb's model as shown in (2) needs to be adapted for implementation. One novelty of this communication consists in proposing an *optimal* approximate scalar (isotropic) viscosity value of the anisotropic 4th order model.

According to (2), for stress computations the viscosity tensor $\mathbb{V}$ is used via its action $\mathbb{V}\mathbf{D}$ on the current deformation rate tensor $\mathbf{D}$. The idea is thus to define an effective scalar viscosity value η_* such that the scalar multiplication $\eta_*\mathbf{D}$ is as close as possible to $\mathbb{V}\mathbf{D}$ in a certain sense. In this paper, we simply use the classical Frobenius norm (square root of the sum of its components) for 2nd order tensors and we minimize the following approximation error

$$\|\eta_*\mathbf{D} - \mathbb{V}\mathbf{D}\|^2 = \min_{v} \|v\mathbf{D} - \mathbb{V}\mathbf{D}\|^2 . \tag{3}$$

Through the Frobenius (elementwise) inner product, the scalar η_* can be simply regarded as the projection of $\mathbb{V}$ in the direction of $\mathbf{D}$. By a direct calculation of (3), we obtain thus the optimal scalar optimal viscosity approximating the Lipscomb's anisotropic one

$$\eta_* = (1 + N_p \mathsf{a}_*)\eta \quad \text{with} \quad \mathsf{a}_* = \frac{\mathbf{D}\cdot\mathbb{A}\mathbf{D}}{\|\mathbf{D}\|^2} = \frac{\mathrm{tr}(\mathbf{D}^T\mathbb{A}\mathbf{D})}{\|\mathbf{D}\|^2}. \tag{4}$$

In (4), the scalar a_* can also be regarded as the optimal equivalent scalar of the 4th order orientation tensor $\mathbb{A}$, for the current deformation rate tensor $\mathbf{D}$ considered.

The computation of this scalar optimal viscosity through (4) requires the 4th order fiber orientation tensor. In general in injection molding simulations it can only be recovered approximately from the 2nd order tensor via a closure formulation. For consistency, we use the same orthotropic closure model described in Verweyst (1998) which is used by default in Moldflow since the version 2017R2.

We recall that in (4), the viscosity η refers to that of the matrix in absence of fibers. In our Moldflow API simulations, it is more convenient to still select the fiber reinforced material (say 50%wt) with a measured viscosity η_{MF}, based on which we will then apply a scaling factor $\hat{\eta}$ incorporating anisotropic effects according to (4). Consequently, we need to recover from η_{MF} at least approximately the viscosity function η corresponding to the non-filled matrix. Since in Moldflow the apparent viscosity η_{MF} is measured using a capillary rheometer at relatively high shear rates, the fibers should be almost perfectly aligned in the shear direction, see Costa et al. (2015). We consider for instance a simple shear flow $\mathbf{v} = x_3\dot{\gamma}\mathbf{e}_1$ in the 1-3 plane. Due to possible fiber-fiber/matrix interactions (see Folgar and Tucker (1984) for instance), the alignment is not perfect and we suppose that the 2nd order fiber orientation tensor can be parametrized by its component in the 1-direction

$$\overline{\mathbf{a}} = \begin{bmatrix} \overline{a}_{11} & & \\ & \frac{1}{2}(1-\overline{a}_{11}) & \\ & & \frac{1}{2}(1-\overline{a}_{11}) \end{bmatrix}, \tag{5}$$

where $\overline{a}_{11}$ should be in general very close to 1 characterizing a quasi unidirectional state. Applying our scalar optimal viscosity (4) for these fiber orientations (5) under the simple shear flow gives

$$\eta_{\mathrm{MF}} = (1 + N_p\overline{\mathsf{a}}_*)\eta , \tag{6}$$

where the function dependence of $\overline{\mathsf{a}}_*$ with respect to $\overline{a}_{11}$ is illustrated in Fig. 1. We verify that for $\overline{a}_{11} = 1$ when the fibers are (somehow indeed) perfectly aligned in the shear direction, the Moldflow apparent viscosity η_{MF} directly gives the matrix viscosity η since in this case fibers have no effect on the suspension viscosity, resulting in $\overline{\mathsf{a}}_* = 0$. For other cases, this small coefficient $\overline{\mathsf{a}}_*$ reflects thus the fiber alignment information contained in the Moldflow fiber reinforced suspension viscosity.

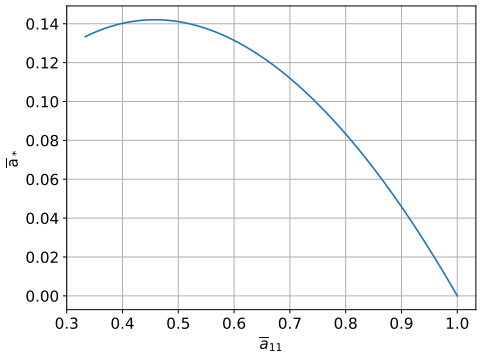

Figure 1: Variation of $\overline{\mathsf{a}}_*$ as $\overline{a}_{11}$ increases from $1/3$ (isotropic state) to 1 (unidirectional state).

Combining (4) et (6), we finally obtain the modified scalar optimal Lipscomb's model that will be implemented in the Moldflow API framework

$$\eta_*(\mathbf{D}, T, p, \mathbf{a}) = \hat{\eta}(\mathbf{D}, \mathbf{a}) \cdot \eta_{\mathrm{MF}}(\dot{\gamma}, T, p) = \frac{1 + N_{\mathrm{p}}\mathsf{a}_*(\mathbf{D}, \mathbf{a})}{1 + N_{\mathrm{p}}\overline{\mathsf{a}}_*}\eta_{\mathrm{MF}}(\dot{\gamma}, T, p). \tag{7}$$

We recall that here $\hat{\eta}$ is the non-dimensional viscosity scaling factor that will be applied to the Moldflow fiber reinforced suspension viscosity η_{MF}. Observe that now the shear rate (tensor) dependence of the resulting semi-anisotropic fiber dependent viscosity η_* is both through the original Moldflow viscosity function (mainly the Cross model) and the coefficient a_* adapting fiber orientation $\mathbf{a}$ induced anisotropy to the current deformation rate tensor $\mathbf{D}$ via (4). The temperature and pressure dependence remain unchanged compared to standard uncoupled simulations.

3. Test-case simulations on a rectangle plate

In this section we intend to investigate numerically the effect of fiber-induced viscosity models presented in Section 2 through injection molding simulations under Autodesk Moldflow. The version Moldflow Insight 2018 is used.

The Moldflow study (`.sdy`) file is kindly provided by the first author of Costa et al. (2015) and we use the same geometry, basic material, injection process and numerical parameters as used in Costa et al. (2015). As can be seen from Fig. 2 (left), the geometry consists of a simple end-gated rectangle flat plate with a thickness of 3.6 mm. Two probe points P1 (near the gate) and P2 (at the plate center) are used to analyze the simulation. The default material parameters of a 50%wt fiber filled polyamide (Zytel PLS95G50DH2 BK261) in the Moldflow database are used, with a standard Cross-WLF viscosity model. The Phan-Thien and Graham (1991)'s N_{p} parameter in the modified Lipscomb's model (7) is computed using the aspect ratio and volume fraction information contained in the Moldflow database, and a fitting parameter $A = 50\%$, which gives $N_{\mathrm{p}} \approx 221$. Since we are mainly interested in the coupling between flow equations and fiber orientations, only a filling simulation without packing phase can be considered. For comparison concerns we

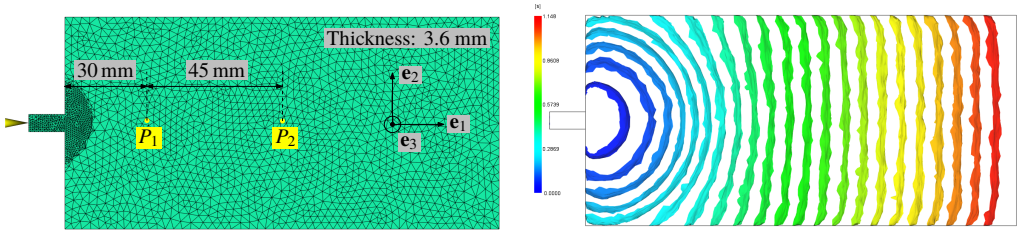

Figure 2: (Left) Rectangle end-gated flat plate with two probe points as used in Costa et al. (2015); (Right) Filling contour for uncoupled injection simulations.

fix a constant ram speed at 50 mm/s which leads to an injection time near 1.15 s. The spatial discretization is realized with sufficiently fine triangles on the surfaces and 16 layers of tetrahedral elements in the gapwise direction.

It will be interesting to evaluate the flow-fiber coupling effects introduced by the fiber-induced viscosity models presented in Section 2, for several fiber orientation models which may contribute differently to the overall coupling. In this communication we will use the two principal fiber orientation models available in Moldflow Insight 2018: the Reduced Strain Closure (RSC) model proposed by Wang et al. (2008) and the lately introduced Moldflow Rotational Diffusion (MRD) model (see Autodesk (2016)). Note that since the Moldflow version 2017R2, the default fiber orientation model becomes the MRD model.

3.1. Fiber orientations predicted by the RSC and MRD models

We will first compare these two fiber orientation models using the default uncoupled viscosity model (Cross-WLF). The default parameters for these fiber models are used. Since the flow equations and the fiber orientation model are uncoupled, the same filling pattern is obtained as illustrated in Fig. 2 (right). Contrary to the experimental results indicated in Costa et al. (2015) where the flow advances faster near the edge than in the center, the simulated contours are essentially convex throughout the filling phase.

The steady a_{11} and a_{13} fiber orientation components in the thickness direction of the probe point P1 are presented in Fig. 3 for both models. At P2 similar results can be obtained and hence are not illustrated here. We recall that the 1-axis corresponds to the horizontal flow direction while the 3-axis is the thickness one, see Fig. 2 (left). The thickness coordinate z is normalized such that -1 (resp. +1) corresponds to the lower (resp. upper) surface and 0 designates the mid-surface. As for the a_{11} component, the well-known skin-shell-core structure can be observed for both fiber models, though the RSC model predicts a more flow-aligned orientation in the shear-dominated shell region. It is also interesting to see that the RSC model gives a larger (yet still small) a_{13} component especially in the shell and skin regions. Note that the trend reported here in Fig. 3 should not be general and only reflects the default parameters set in Moldflow.

3.2. Coupled simulations using the MRD fiber model

We first test modified Lipscomb model (7) using the MRD fiber model. The a_{11} variation in the thickness for both probe points are presented in Fig. 4. At P1, Lipscomb's model predicts a widened fiber core region compared to the uncoupled case due to the flow-fiber coupling. It also shows a slightly more orientated shell region. At P2, fibers are somehow predicted to be more aligned in the flow direction compared to the uncoupled model. Nevertheless the fiber orientation still displays a plausible skin-shell-core structure.

The velocity profile and viscosity at P1 are then analyzed in Fig. 5 to evaluate the effect of flow-fiber coupling on kinematics and rheological properties. It can be seen from Fig. 5 (left) that compared to the uncoupled case, the velocity profile is now essentially flattened (plug flow) in the core region resulting from

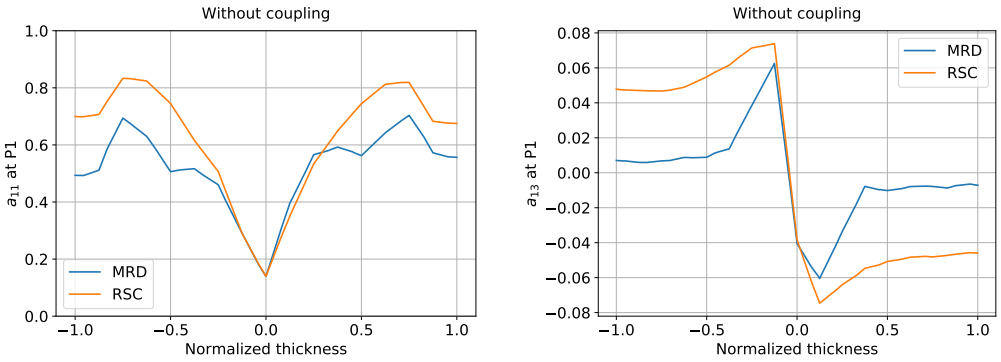

Figure 3: Fiber orientation a_{11} (left) and a_{13} (right) components at P1 for both MRD and RSC models without viscosity coupling effects.

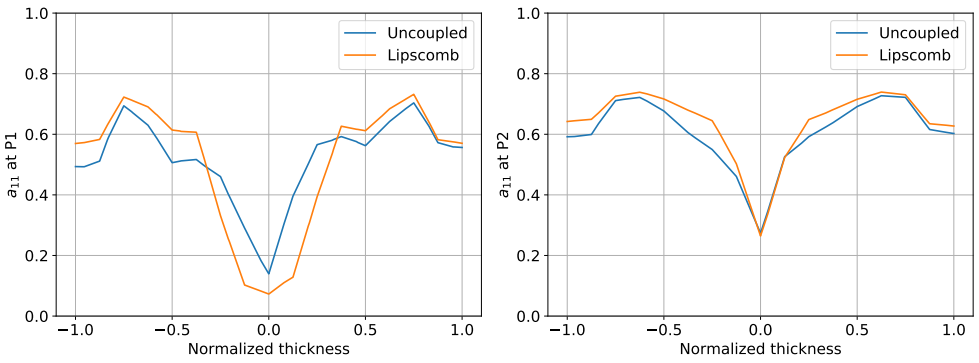

Figure 4: Fiber orientation a_{11} component at P1 (left) and P2 (right) probe points with the MRD model for the modified Lipscomb model with $\overline{a}_{11} = 0.93$.

the corresponding viscosity increase (by a factor of 10 at the center) as indicated in Fig. 5 (right). The overall deformation rate is thus significantly reduced in that region, which explains a less aligned core in Fig. 4 (left). Since the probe point P1 is near the gate, we suspect that this fiber-induced increased viscosity should originate from an elongational flow in the transverse direction. This point will be verified in the next section.

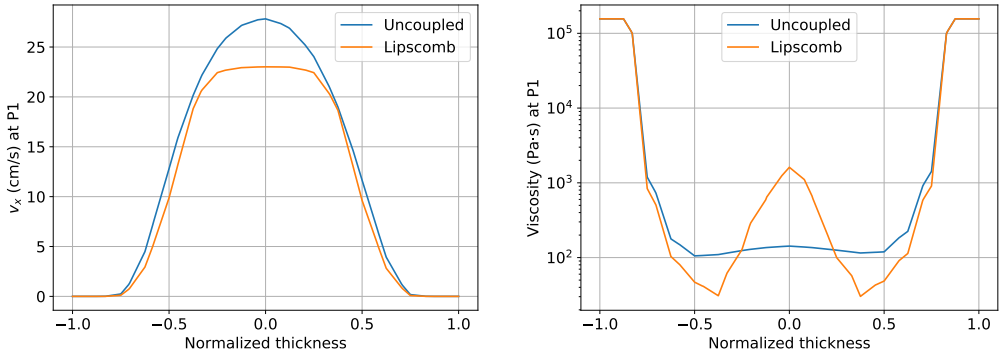

Figure 5: Results obtained at the end of filling at P1 with the MRD model for the modified Lipscomb model with $\overline{a}_{11} = 0.93$: (Left) Velocity profile v_x; (Right) Viscosity profile.

Concerning the overall filling pattern when using the modified Lipscomb's model (7), it is essentially the same as that illustrated in Fig. 2 for the uncoupled case. Further work will be devoted to investigating why it fails to predict a locally concave contour as shown in Costa et al. (2015).

3.3. Coupled simulations with the RSC model

Now the flow-fiber coupling effects introduced by the modified Lipscomb's model (7) will be evaluated for the RSC model. Again we first compare the fiber orientation profile at both probe points for the coupled and uncoupled cases. For the $\overline{a}_{11}$ parameter characterizing fiber alignment in the Moldflow viscosity (see Fig. 1), two values are tested. According to Fig. 6, fiber orientation is not very sensitive to the $\overline{a}_{11}$ parameter. Interestingly, compared to the MRD case (Fig. 4), now for both probe points we have a slowed down fiber alignment throughout the thickness and consequently a widened fiber core region. This indicates that different fiber models may also contribute differently to the overall coupling effect.

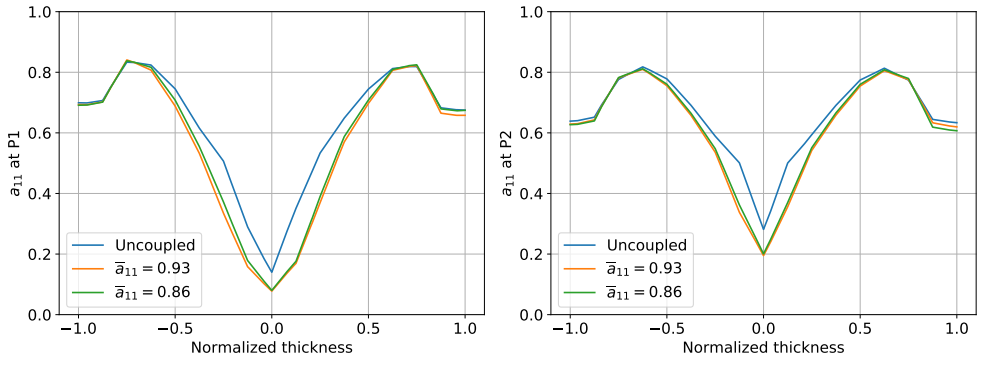

Figure 6: Fiber orientation a_{11} at P1 (left) and P2 (right) with the RSC model for the modified Lipscomb model.

In Figs. 4 and 6, only the final fiber orientation states at the end of filling are presented. It will also be interesting to analyze temporal fiber evolutions for both coupled and uncoupled models. The averaged (in the thickness direction) fiber orientation as a function of filling time is illustrated in Fig. 7. It can be observed that the temporal fiber orientation increases monotonically. Due to flow-induced viscosity increase, the overall deformation rate is reduced implying a systematic slowed down fiber alignment.

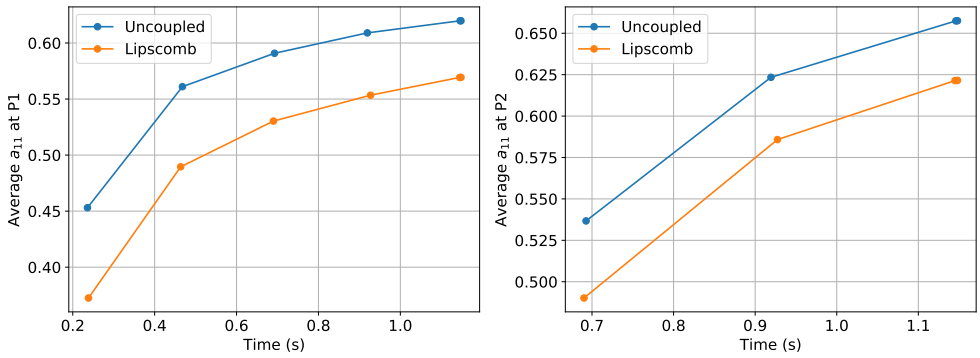

Figure 7: Temporal evolution of the average a_{11} in the thickness at P1 (left) and P2 (right) with the RSC model for the modified Lipscomb model $\overline{a}_{11} = 0.86$.

Now, we will investigate what exactly happened at these two probe points P1 and P2 that leads to what we observe in Figs. 4 to 7. For that, we need to analyze the deformation rate tensor $\mathbf{D}$ in the thickness direction. Since the tensor components of $\mathbf{D}$ are not directly available in Moldflow, the velocity field $\mathbf{v}$ at the end of fill is exported through a home-made script to another post-processing software, where the gradient of $\mathbf{v}$ can be automatically computed. To make sure that our computation of $\mathbf{D} = \frac{1}{2}\,\mathrm{dev}(\nabla\mathbf{v} + \nabla^{\mathsf{T}}\mathbf{v})$ matches that of Moldflow, the generalized shear rate $\dot{\gamma} = \sqrt{2}\,\|\mathbf{D}\|$ is first compared in Fig. 8 (left). The shear rate given by Moldflow can be indeed accurately recovered, which validates our post-processing approach.

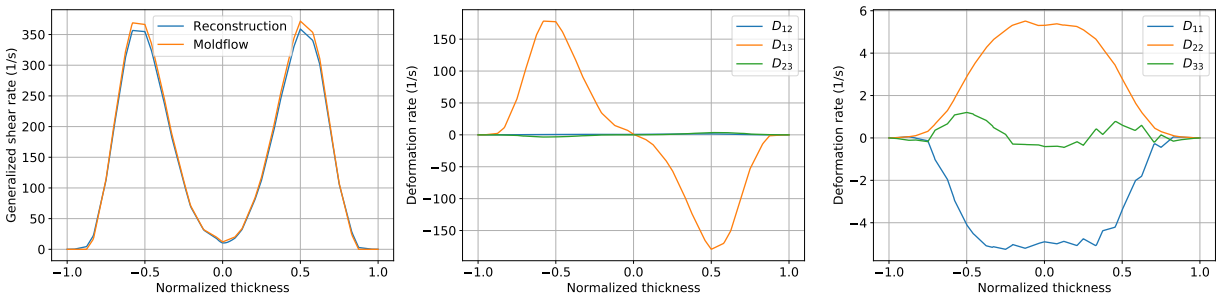

Figure 8: Deformation rate at P1 with the RSC model for the modified Lipscomb model at $\overline{a}_{11} = 0.93$: (left) generalized scalar shear rate, (center) shear components and (right) elongational components.

It can be seen from Fig. 8 (center) that the 13 shear component is dominant compared to other shear components, which is fairly typical for thin-walled injection molding, see Tucker (1991). According to Fig. 8 (right), a planar elongational flow toward the transverse direction is indeed observed especially on the

mid-surface $z = 0$ at P1, where the deformation rate tensor is given by

$$\mathbf{D} = \begin{bmatrix} -4.9 & 0.8 & 0.9 \\ 0.8 & 5.3 & 0 \\ 0.9 & 0 & -0.4 \end{bmatrix} 1/\mathrm{s}.$$

It indicates that at P1, the core region is dominated by a divergent (uniaxial transverse extensional) flow. Using the reconstructed deformation rate tensor in Fig. 8 (center and right) and the fiber orientation tensors, the analytical formula of the modified Lipscomb's model (7) can be applied. The thus obtained theoretic viscosity scaling factor is compared to Moldflow results in Fig. 10 (left). A relatively good agreement can be found between them, which hence validates our implementation of (7) in the Moldflow Insight API framework. The slight discrepancy may mainly originate from the exact calculation of the deformation tensor and especially different averaging operators in Moldflow and our post-processing. At the mid-surface a viscosity scaling factor near 10 is retrieved (see Fig. 5). This illustrates that it is indeed the planar extensional flow in the 2 direction that is mainly responsible for the viscosity increase in the core region.

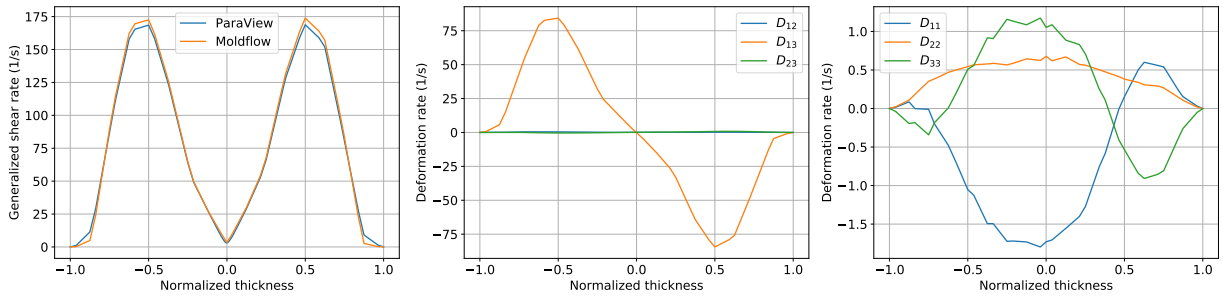

Figure 9: Deformation rate at P2 with the RSC model for the modified Lipscomb model at $\overline{a}_{11} = 0.93$: (left) generalized scalar shear rate, (center) shear components and (right) elongational components.

The above analyses are now applied to the probe point P2 in Fig. 9. This time the deformation rate tensor at the mid-surface is now given by

$$\mathbf{D} = \begin{bmatrix} -1.7 & 0.1 & -0.2 \\ 0.1 & 0.7 & 0.1 \\ -0.2 & 0.1 & 1.1 \end{bmatrix} 1/\mathrm{s}.$$

It can be observed that at P2 we no longer have a planar divergent flow but a biaxial extensional flow toward the 2-3 directions in the core region. Furthermore, in terms of magnitude it is also not comparable to that observed at P1. It must be something else that contributes primarily to a widened fiber orientation core observed in the RSC model at P2, see Fig. 6 (right). In Fig. 10 (right), we compare the viscosity scaling factor obtained with the MRD and the RSC model. Although at the mid-surface the MRD gives a slightly larger value, the RSC model presents a larger overall value in the whole thickness. Since the 13 shear component is dominant almost throughout the thickness except very near the mid-surface, the flow-fiber coupling should mainly come from the fibers oriented in that plane. According to Fig. 3 (right), by default the RSC model predicts indeed more fiber orientations in the 13 plane than the MRD model. In the authors' opinion this maintains the overall viscosity in the shell region with the RSC model, and in the same time widens the core region in Fig. 6 (right) due to a scaling factor still larger than 1 in the core gion.

Finally, in Fig. 11, we compare the pressure temporal evolution at the injection point, for two values of $\overline{a}_{11}$. A larger value (closer to 1) of $\overline{a}_{11}$ leads to an overestimated evolution compared to the uncoupled

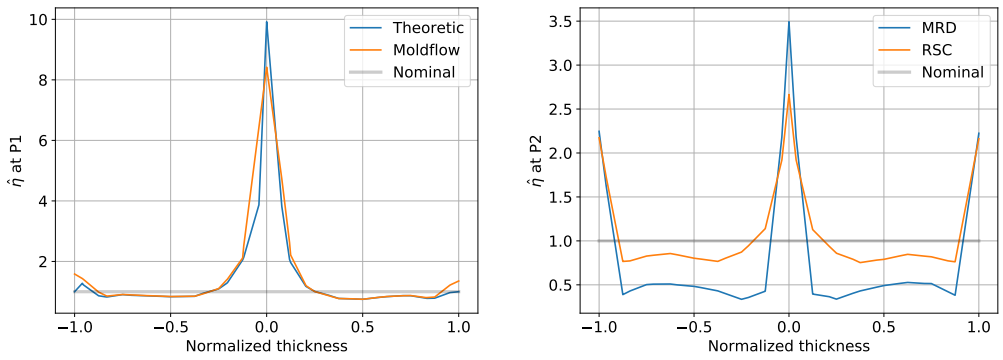

Figure 10: Viscosity scaling factor for the modified Lipscomb model at $\overline{a}_{11} = 0.93$: (left) comparison at P1 between theoretic and Moldflow values with the RSC model; (right) comparison between the MRD and RSC fiber models at P2 (Moldflow calculations)

case. This agrees well with our definition in (7) since in the limiting case $\overline{a}_{11} = 1$, we have $\overline{\mathsf{a}}_* = 0$ and the uncoupled Moldflow viscosity is assumed to be that of the unfilled matrix, based on which we will apply then a scaling factor $1 + N_{\mathrm{p}}\mathsf{a}_*$ always bigger than 1. This may very likely increase the overall pressure prediction. The use of a smaller $\overline{a}_{11}$ assumes that fibers are not perfectly aligned during the Moldflow measurement of viscosity, and compensates the pressure prediction. This parameter $\overline{a}_{11}$ can thus be regarded as a fitting parameter of the model.

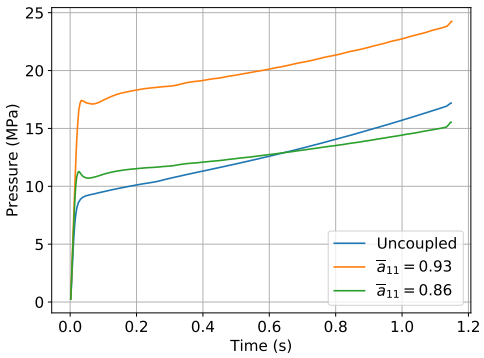

Figure 11: Pressure at the injection point with the RSC model for the modified Lipscomb model.

4. Conclusions and future work

From rheological modeling of fiber-reinforced suspension point of view, this paper proposed a modified yet *optimal* version (4) of the original Lipscomb's model that reduces an anisotropic 4th order tensor to a scalar, even though it was initially motivated by computational implementation purposes. According to coupled simulation results presented in Section 3, the modified scalar Lipscomb's model (7) performs equally well compared to the original one and successfully captures elongational flows and fiber orientation components in the dominating shear plane.

Via these fiber-dependent viscosity models, flow kinematics and fiber evolutions are now tightly two-way coupled through rheological properties. In particular, a slowed down fiber alignment in the flow direction with a widened core region can be obtained, depending directly on the particular local deformation conditions

and fiber states. Using the modified Lipscomb's model (7), it is expected that the extensional flows will be better taken into account especially in the core region. Fiber orientation prediction for geometrically complex chunky parts Kleindel et al. (2015) could be improved.

In this paper, the flow-fiber coupling effects are evaluated by two latest fiber orientation models available in Moldflow. Since once established the coupling works both ways, different fiber models may deliver different contributions to overall flow-fiber coupling. Attention must be taken when comparing results of coupled simulations with different orientation models. According to our results in Section 3, it seems that the RSC model results in more coupling effects than the newly introduced MRD model. Note that this conclusion may only be limited to the behaviors using default parameters.

This paper reports some of the preliminary results of our research on fiber-induced viscosity modeling. It will be followed by additional communications that may include the following interesting theoretical and practical aspects:

- Theoretic rheological analyses and computational details of the modified viscosity model (7): comparison with the original model in terms of approximation errors, implementation in the Moldflow Insight API framework, computation efficiency[1]. . .
- Accounting for other additional fiber-induced rheological contributions. Different coupling may exist between flow equations and fiber evolution models, as indicated in Fig. 12. In this paper only orientation effects are considered. Future work could be for instance devoted to the coupling effects introduced by a non-homogeneous volume fraction distribution, which itself is predicted by a fiber migration model such as Morris (2009).

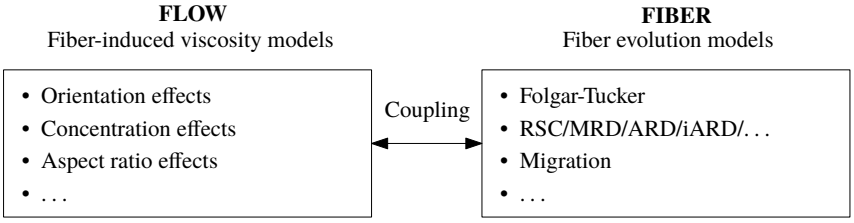

Figure 12: Coupling between flow equations and fibers through fiber-induced viscosity models.

- Implications of coupled injection molding simulations in subsequent integrative mechanical simulations that take into account the previous processing results: how the stress distribution is varied by using a fiber-flow coupling injection simulation;
- Experimental validation of the proposed flow-fiber coupled simulations on structural parts.

Acknowledgement

The work presented in this document is financially supported by the THERMOFIP research program coordinated by Solvay Engineering Plastics. The authors would like to express again their sincere gratitude to Autodesk Moldflow developers and in particular Dr. Franco Costa for his guidance and valuable comments. Also, the Moldflow API simulations presented in Section 3 can not be performed without the kind and generous help of Alain Benchissou from APLICIT.

[1]Contrary to what may have been suggested in Kleindel et al. (2015), coupled injection simulations are not so costly according to our experiences.

Competing interests

The authors declare that they have no competing interests.

References

Adam, L., Assaker, R., 2014. Integrated nonlinear multi-scale material modelling of fiber reinforced plastics with Digimat: Application to short and continuous fiber composites. In: Proceedings of the 11th World Congress on Computational Mechanics. pp. 20–25.

Advani, S. G., Tucker, C. L., 1987. The use of tensors to describe and predict fiber orientation in short fiber composites. Journal of Rheology 31 (8), 751–784.

Autodesk, 2016. Fiber orientation accuracy validation report for Moldflow Insight 2017 R2.

Costa, F., Cook, P., Pickett, D., 2015. A framework for viscosity model research in injection molding simulation, including pressure and fiber orientation dependence. In: SPE ANTEC Conference.

Folgar, F., Tucker, C. L., 1984. Orientation behavior of fibers in concentrated suspensions. Journal of reinforced plastics and composites 3 (2), 98–119.

Kleindel, S., Salaberger, D., Eder, R., Schretter, H., Hochenauer, C., 2015. Prediction and validation of short fiber orientation in a complex injection molded part with chunky geometry. International Polymer Processing 30 (3), 366–380.

Laun, H. M., 1984. Orientation effects and rheology of short glass fiber-reinforced thermoplastics. Colloid & Polymer Science 262 (4), 257–269.

Lipscomb, G. G., Denn, M. M., Hur, D. U., Boger, D. V., 1988. The flow of fiber suspensions in complex geometries. Journal of Non-Newtonian Fluid Mechanics 26 (3), 297–325.

Mazahir, S., Vélez-García, G., Wapperom, P., Baird, D., 2013. Evolution of fibre orientation in radial direction in a center-gated disk: Experiments and simulation. Composites Part A: Applied Science and Manufacturing 51, 108–117.

Morris, J. F., 2009. A review of microstructure in concentrated suspensions and its implications for rheology and bulk flow. Rheologica acta 48 (8), 909–923.

Papathanasiou, T. D., 1997. Flow-induced alignment in composite materials. Woodhead Publishing Cambridge, Ch. Flow-induced alignment in injection molding of fiber-reinforced polymer composites.

Phan-Thien, N., Graham, A., 1991. A new constitutive model for fibre suspensions: flow past a sphere. Rheologica acta 30 (1), 44–57.

Phan-Thien, N., Zheng, R., 1997. Flow-induced alignment in composite materials. Woodhead Publishing Cambridge, Ch. Macroscopic modelling of the evolution of a fibre orientation during flow.

Ranganathan, S., Advani, S. G., 1993. A simultaneous solution for flow and fiber orientation in axisymmetric diverging radial flow. Journal of Non-Newtonian Fluid Mechanics 47, 107–136.

Redjeb, R., Silva, L., Laure, P., Vincent, M., Coupez, T., 2006. Three dimensional numerical simulations of fiber orientation in injection molding. In: 9th ESAFORM.

Rolland, H., Saintier, N., Robert, G., 2016. Damage mechanisms in short glass fibre reinforced thermoplastic during in situ microtomography tensile tests. Composites Part B: Engineering 90, 365–377.

Tseng, H.-C., Chang, R.-Y., Hsu, C.-H., 2017. Improved fiber orientation predictions for injection molded fiber composites. Composites Part A: Applied Science and Manufacturing 99, 65–75.

Tucker, C. L., 1991. Flow regimes for fiber suspensions in narrow gaps. Journal of Non-Newtonian Fluid Mechanics 39 (3), 239–268.

Verweyst, B. E., 1998. Numerical predictions of flow-induced fiber orientation in three-dimensional geometries. Ph.D. thesis, University of Illinois at Urbana-Champaign.

Verweyst, B. E., Tucker, C. L., 2002. Fiber suspensions in complex geometries: Flow/orientation coupling. The Canadian Journal of Chemical Engineering 80 (6), 1093–1106.

Vincent, M., Giroud, T., Clarke, A., Eberhardt, C., 2005. Description and modeling of fiber orientation in injection molding of fiber reinforced thermoplastics. Polymer 46 (17), 6719–6725.

Wang, J., O'Gara, J. F., Tucker, C. L., III, 2008. An objective model for slow orientation kinetics in concentrated fiber suspensions: Theory and rheological evidence. Journal of Rheology 52 (5), 1179–1200.

Wedgewood, A., Zhang, Z., Sulmoni, M., Kang, S., 2017. Addressing practical challenges in developing Digimat material laws. In: Digimat Users' Meeting, Berlin, Germany.